

Effects of Length and Diameter of Open-Ended Coaxial Sensor on its Reflection Coefficient

K. Y. YOU¹, J. SALLEH¹, Z. ABBAS²

¹ Dept. of Radio Communication Engineering, Faculty of Electrical Engineering, Universiti Teknologi Malaysia, 81310 UTM Skudai, Malaysia

² Dept. of Physics, Faculty of Science, Universiti Putra Malaysia, 43400 UPM Serdang, Malaysia

kyyou@fke.utm.my, jamaliahsalleh@ymail.com, za@fsas.upm.edu.my

Abstract. This paper presents a calibration technique for a coaxial sensor using a transmission signal approach. The sensor was fabricated from commercially available RG402/U and RG405/U semi-rigid coaxial cable. The length of the coaxial sensor was correlated with the attenuation and standing wave inside the coaxial line. The functions of multiple reflection amplitude and tolerance length with respect to the actual length of coaxial line were empirically formulated using regression analysis. The tolerances and the undesired standing wave which occurs along the coaxial line were analyzed in detail.

Keywords

Long open-ended coaxial sensor, aperture calibration, standing wave, transmission line, tolerance length, semi-rigid coaxial cable.

1. Introduction

Recently, narrow and long coaxial line probes have been widely used for *in vivo* medical treatment to detect malignant tissues in the human body. This type of probe is very useful to measure small amounts of samples placed in a depth container. However, measurements using a long open ended coaxial line will produce a significant standing wave inside the coaxial line, due to the superposition between the incident wave and the reflected wave. In this work, two long coaxial sensors were fabricated and tested using a network analyzer. The relationship between the length of coaxial probe and the standing wave properties was observed. This is represented by (1) and (2), using a rigorous transmission model. The standing wave amplitudes, tolerance length and the attenuation factor in (1) and (2) were found and expressed in terms of the actual length d of the coaxial probe using regression analysis. Finally, the aperture coaxial sensor can be calibrated efficiently by removing the standing wave and the attenuation along the coaxial line using (1) and (2).

2. Transmission Wave in Coaxial Line

In an ideal coaxial line, the magnitude of the transmitted polar wave is always constant and its phase, ϕ , is shifted exponentially, $\exp(j\phi)$. Practically, the conductors and the dielectric material in the coaxial line will cause attenuation in the wave when it is propagated. Moreover, mismatches may occur at the joint between the connector plug and the coaxial cable (due to the tolerance in the dimension) caused by the material between the plug and the semi-rigid coaxial cable.

Fig. 1 shows the configuration of the sensor and the transmission network inside a coaxial line. The incident wave from the plane AA' is transmitted to the plane BB' by the shifting phase of $k_c d$, and is reflected back to input AA' with the same shifting phase. Thus, the aperture reflection coefficient, $\Gamma_{BB'}$ at the plane BB' can be found by the phase delay of $2k_c d$ with respect to the measured $\Gamma_{AA'}$ at the plane AA' . The relationship is given as $\Gamma_{BB'} = \Gamma_{AA'} \exp(2jk_c d)$. However, the transmission line is imperfect, and a fringing field occurs near the aperture sensor. Hence, a phase shift between the forward wave and the reflected wave occurs, and produces the standing wave inside the coaxial line. Fig. 1 also shows the propagation of the electric field contour. For a long coaxial line, the ripple in the broad frequency range measurement is higher, and this ripple condition has been deduced due to repeated change in the polarization direction of the electric field, which increased when the coaxial length was increased.

Fig. 2 illustrates a corresponding vector diagram for the only real part of the reflection coefficient, $\text{Re}(\Gamma_{BB'})$. The solid blue line to the radius of the circle represents the magnitude of $\text{Re}(\Gamma_{AA'})$ at the plane AA' . The dashed blue line shows the real part of the reflection coefficient at the BB' after delaying the phase of $2k_c d$ from the plane AA' . The reflection coefficient at BB' is slightly increased, due to the conductor and dielectric loss in the coaxial line.

The magnitude of $\text{Re}(\Gamma_{AA'})$ is affected by the imaginary part of the reverse reflected wave, $\rho_0 |\text{Im}(\Gamma_{AA'})|$ which is represented by a solid red line, and its direction is

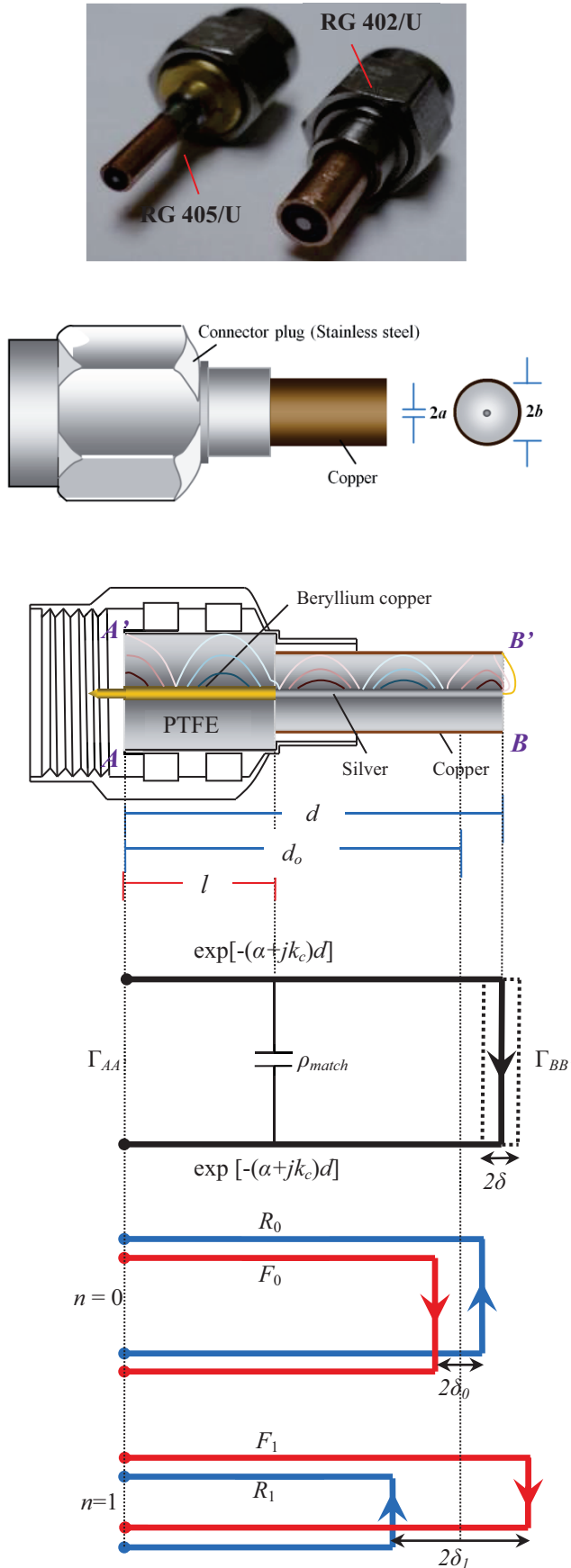


Fig. 1. Configuration of fabricated semi-rigid coaxial sensor and the transmission network calibration.

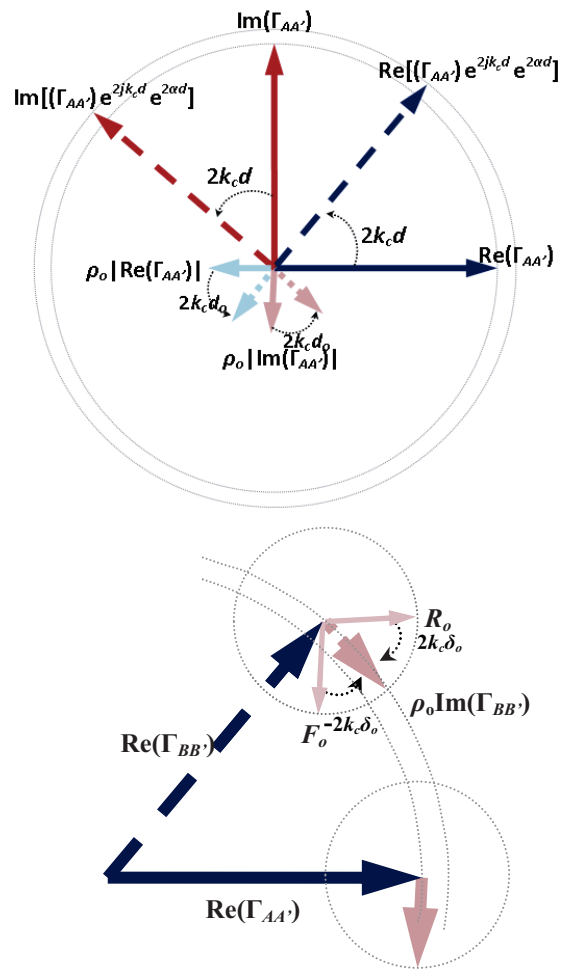


Fig. 2. Vector diagram for real part of reflection coefficient, $Re(\Gamma_{meas})$ along transmission network.

perpendicular to $Re(\Gamma_{AA'})$. Similarly, the $\rho_0|Im(\Gamma_{AA'})|$ at AA' can be de-embedded to the aperture, BB' , by the shifting phase of $2k_c d_0$. The ρ_0 is the first order of the reverse factor for the imaginary part of the reflection coefficient and its value is determined based on measurement (see Tab. 1). The reverse reflected wave is the mismatch error mainly caused by fringing field effects (stray capacitive effects) at the open end of the coaxial line. The propagated wave in the coaxial line is in polar form, thus the changes in the real and imaginary parts of the polar wave are the reciprocal linkages. When the direction of $\rho_0|Im(\Gamma_{AA'})|$ is exactly perpendicular to $Re(\Gamma_{AA'})$, there is no change in the magnitude of $Re(\Gamma_{AA'})$. Conversely, if $\rho_0|Im(\Gamma_{AA'})|$ and $Re(\Gamma_{AA'})$ are not perpendicular to the other, then the combined vector of both will result in either an increase or decrease in the magnitude of $Re(\Gamma_{AA'})$. As mentioned earlier, the sum of the forward wave and the reflected wave created a standing wave in the coaxial line which only oscillates in instantaneous magnitude without propagating through the length of the coaxial line. Hence, the interference from the phase shift between the forward wave and the reflected wave along the coaxial line causes the $Re(\Gamma_{meas})$ to oscillate periodically with frequency. The changing direction of the oscillation is dependent on

whether the interference is destructive or constructive, at a certain frequency (See Appendix). In order to facilitate the sketching, Figs. 1 and 2 show the basic concept of the wave propagation and the interference that occurs in the coaxial line. This is not completely representative of the actual state of the coaxial line. In fact, the wave propagation in the coaxial line involves a series of interferences.

The imaginary part of the reflection coefficient, $\text{Im}(\Gamma_{BB'})$, can also be observed in a similar way. Thus, the measured $\Gamma_{BB'} = \text{Re}(\Gamma_{BB'}) + j\text{Im}(\Gamma_{BB'})$ at the BB' is obtained by

$$\text{Re}(\Gamma_{BB'}) = \text{Re}(A) + |\text{Im}(A)| \times \text{Re}(B), \quad (1)$$

$$\text{Im}(\Gamma_{BB'}) = \text{Im}(A) + |\text{Re}(A)| \times \text{Im}(B) \quad (2)$$

where

$$A = \Gamma_{AA'} \exp(2jk_c d) \exp(2\alpha d') \rho_{\text{match}}, \quad (3a)$$

$$B = \sum_{n=0}^{\infty} (-1)^n \exp(2jk_c d_n) \{ \rho_n^+ \exp[-2jk_c \delta_n (-1)^n] - \rho_n^- \exp[2jk_c \delta_n (-1)^n] \}, \quad (3b)$$

$$\rho_{\text{match}} = \exp(\zeta \sqrt{f} + 2jk_c \delta) \quad (3c)$$

where the function A is the transmission wave along the coaxial line. k_c is the coaxial line propagation constant. Function B is due to the standing wave along the coaxial line. The ρ_n^+ and ρ_n^- are the amplitude of the n order forward, F_n and backward, R_n multiple reflection respectively along the coaxial line. In practice, at least two terms of B series ($n=0$ and $n=1$) will be sufficiently accurate to formulate the standing wave when the plug and coaxial cable are perfectly connected. From (3b), the $n=0$ and $n=1$ order of forward and backward reflection (F_0, F_1, R_0, R_1), as shown in Fig. 1, are written as

$$F_0 = \rho_0^+ \exp[2jk_c (d_0 - \delta_0)], \quad (4a)$$

$$R_0 = -\rho_0^- \exp[2jk_c (d_0 + \delta_0)], \quad (4b)$$

$$F_1 = \rho_1^+ \exp[2jk_c (d_1 + \delta_1)], \quad (4c)$$

$$R_1 = -\rho_1^- \exp[2jk_c (d_1 - \delta_1)]. \quad (4d)$$

The sum of the values of $(\rho_0^+ + \rho_0^-)$ represents the maximum amplitude of the main standing wave at certain positions of $(d_n \pm \delta_n)$ in the coaxial line. While, the sum of the values of $(\rho_1^+ + \rho_1^-)$ is the amplitude of the other standing wave which is caused by secondary interference in the coaxial line. The transmission line losses can be contributed to the exponential term of $\exp(2\alpha d')$, where α is the attenuation factor along the coaxial line (in Neper/meter). The attenuation $\alpha d'$, is given as [4]

$$\alpha d' = \frac{\sqrt{\pi \epsilon_0 \epsilon_c f}}{2 \ln(b'/a') \sqrt{\sigma_{\text{BeCu}}}} \left(\frac{1}{a'} + \frac{1}{b'} \right) + \frac{\sqrt{\pi \epsilon_0 \epsilon_c f}}{2 \ln(b/a)} \left(\frac{1}{a \sqrt{\sigma_{\text{Si}}}} + \frac{1}{b \sqrt{\sigma_{\text{Cu}}}} \right) (d-l) \quad (5)$$

where σ_{Si} (Silver: 6.14×10^7 S/m) and σ_{Cu} (Copper: 5.88×10^7 S/m) are the conductivities for the inner and outer of conductors, respectively, and σ_{BeCu} (Beryllium copper: 1.72×10^7 S/m) is the conductivity of the plug conductor [3]. The symbol l is the coaxial length in the plug connector and f is the operating frequency. The dimension d (in meters) is the actual length of the coaxial line. The reflection, ρ_{match} is due to the slotted contacts having different mating pin diameters and material between the plug and the coaxial cable. The ζ and δ are, respectively, the loss constant and the tolerance phase shifted length due to the discontinuities. The parameters $(\delta, \zeta, d_n, \delta_n, \rho_n^+$ and $\rho_n^-)$ are obtained by optimization between the measured $\Gamma_{AA'}$ at the plane AA' and the finite element simulation results at the plane BB' . The relationship between these parameters and the coaxial length, d , is created by regression analyses. Finally, the optimized parameters are expressed as a function of d , as listed in Tab. 1.

3. Experimental Setup and Measurement

The reflection coefficient, $\Gamma_{BB'}$ at the aperture sensor (plane BB') can be obtained after calibration using (1) and (2). The reflection coefficient, $\Gamma_{BB'}$ was measured using the fabricated RG402/U and RG405/U semi rigid PTFE-filled ($\epsilon_c = 2.03 \pm 0.01$) coaxial sensors, with an Agilent E5071C Network Analyzer, with frequency over 300 MHz to 20 GHz at $(25 \pm 1)^\circ\text{C}$. For the RG 402/U sensor, the outer radius of the inner conductor is $a = 0.455$ mm, and inner radius of the outer conductor, $b = 1.49$ mm. While the RG 405/U sensor has $a = 0.255$ mm and $b = 0.838$ mm. Both sensors were fabricated with the 3.5 mm SMA male connector, which has $l = 3$ mm with $a' = 0.65$ mm and $b' = 2.05$ mm. Before the measurements, calibrations were performed at the end of the plane AA' , using Agilent 85052D kits. Finally, various lengths, d (15 mm to 130 mm), of both coaxial sensors were measured, respectively.

4. Results and Discussion

4.1 Loss in Coaxial Line

Figs. 3 and 4 show the measured magnitude of reflection coefficient, $|\Gamma_{AA'}|$ for various lengths, d , of coaxial sensor, of which the ends are open to the air. The ripple of $|\Gamma_{AA'}|$ due to the multiple reflection in the coaxial line is more obvious for the longer coaxial line than the shorter, for both coaxial probes. In fact, for RG 402/U and RG405/U which have the same length, the number of ripples is similar for both coaxial probes covered in the frequency range. From the measurement, the average reflection losses are 0.005/cm and 0.0035/cm at 10 GHz, for the RG405/U and the RG402/U coaxial lines respec-

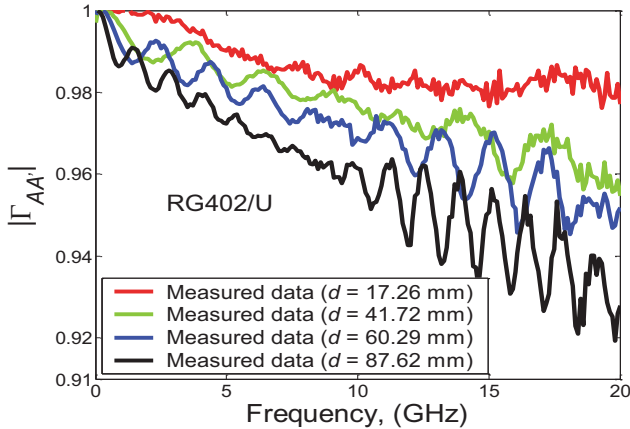


Fig. 3. Measured $|\Gamma_{AA'}$ for air at plane AA' using RG 402/U sensor.

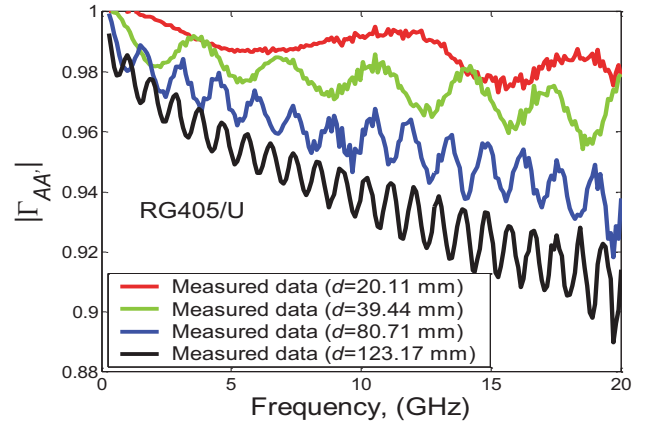


Fig. 4. Measured $|\Gamma_{AA'}$ for air at plane AA' using RG 405/U sensor.

tively. The variations in calculated attenuation, ad' using (4) with frequency are plotted in Fig. 5. As expected, these attenuations are proportional to the root square of frequency, $f^{1/2}$. Overall, the narrower RG 405/U has higher attenuation, when compared to the RG 402/U, for arbitrary corresponding coaxial lengths. Besides the conductor loss, the dielectric loss also slightly affects the propagation wave inside the coaxial line. But, until now, there are no complete values of dielectric constant, ϵ_c for PTFE at a certain range of frequency. We assumed that the ϵ_c varies based on the Debye polarization trend from 300 MHz to 20 GHz, and its parameters are fitted as $\epsilon_\infty = 2.03$, $\epsilon_s = 2.04$ and $\tau = 65$ ps.

4.2 Discontinuity in Coaxial Line

At least two discontinuities occurred along the coaxial line. One is at the contact area between the connector plug and the coaxial cable. The other is the discontinuity at the open end of the coaxial line. In this study, the mismatches were corrected by (3c). The tolerance length δ versus the coaxial length d for both sensors, which were calculated from polynomial equations in Tab. 1, was plotted in Fig. 6. It was deduced that the δ were mainly contributed to by the junction connection, since the values of δ are near to the length of SMA plug connector ($l = 3$ mm). The ζ and δ were expressed as a function of d (see Tab. 1). The results in Tab. 1 show that $\rho_o^+ = 0.105$ and $\rho_o^- = 0.095$ for RG402 means that the maximum of SWR is approximated as 1.2.

4.3 Standing Wave in Coaxial Line

If the function B in (1) and (2) is neglected, a significant noise in the measured $\Gamma_{BB'}$ will give a mean relative error up to 47 % and 74 % for both sensors, when compared to the simulation results, as shown in Figs. 7 and 8. Figs. 9, 10, 11 and 12 show the measured $\Gamma_{BB'}$ for air and water by considering the standing wave. It is evident that the oscillating noise which occurred in the measured $\Gamma_{BB'}$

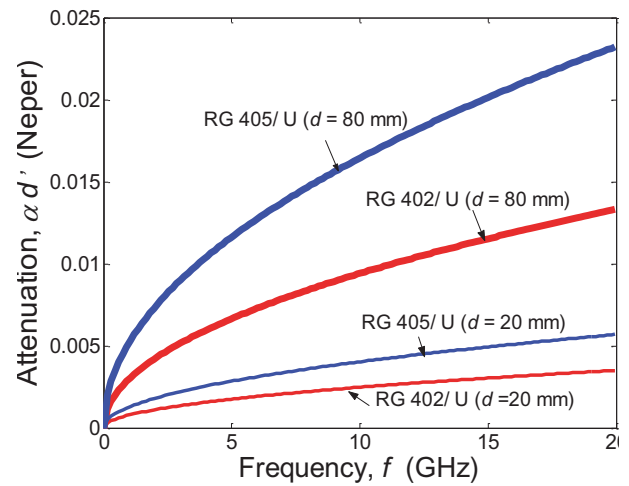


Fig. 5. Variation in ad' with frequencies.

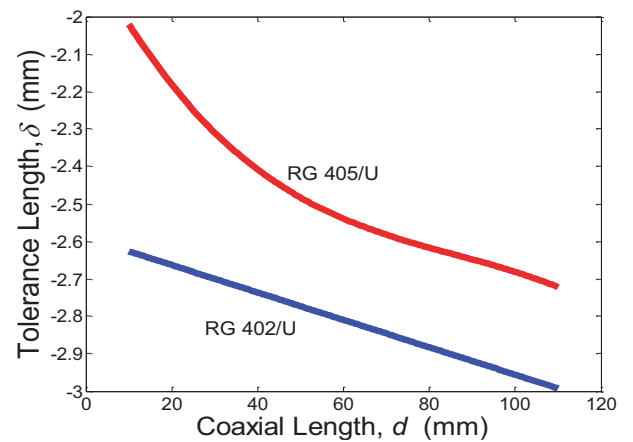


Fig. 6. Variation in tolerance δ with coaxial length, d .

RG 402 Coaxial Probe	$d_o = d_i = (d - 0.0059999)$ $\zeta = 9.4214 \times 10^{-7} d + 7.747 \times 10^{-8}$ $\delta = -3.6581 \times 10^{-3} d - 2.590 \times 10^{-3}$ $\delta_o = 0.0012$; $\delta_i = 0.0045$ $\rho_o^+ = 0.105$; $\rho_o^- = 0.095$ $\rho_i^+ = 0.04$; $\rho_i^- = 0.035$
RG 405 Coaxial Probe	$d_o = d_i = (d - 0.0072603)$ $\zeta = 2.3264 \times 10^{-6} d + 7.8718 \times 10^{-8}$ $\delta = -0.85708 d^3 + 0.22167 d^2 - 0.022221d - 0.0018189$ $\delta_o = -0.0015$; $\delta_i = -0.0012$ $\rho_o^+ = 0.098$; $\rho_o^- = 0.1$ $\rho_i^+ = 0.046$; $\rho_i^- = 0.05$

Tab. 1. The parameters in (1) and (2) for RG 402/U and RG 405/U sensors.

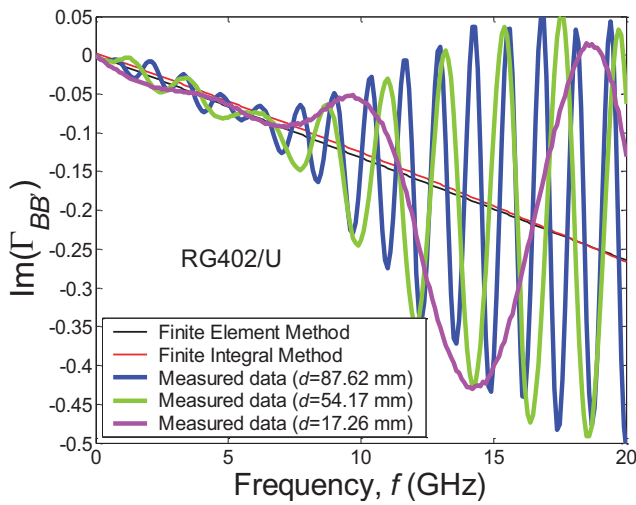


Fig. 7. Measured $\Gamma_{BB'}$ for air without considering standing wave for RG 402/U.

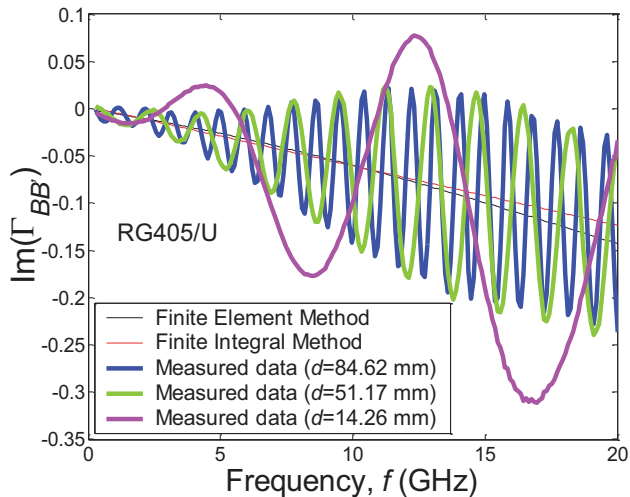


Fig. 8. Measured $\Gamma_{BB'}$ for air without considering standing wave for RG 405/U.

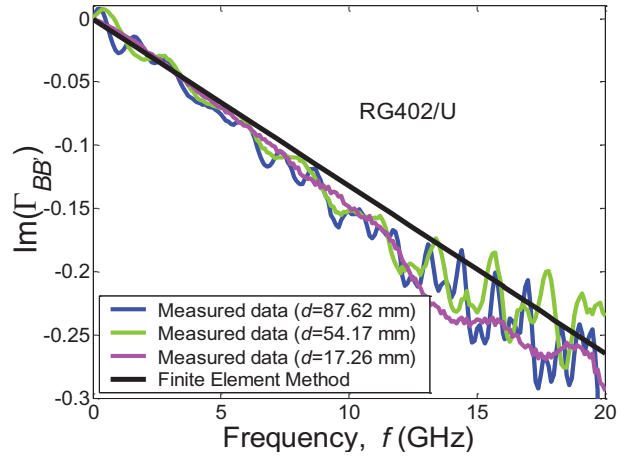


Fig. 9. Measured $\Gamma_{BB'}$ for air with considering standing wave for RG 402/U.

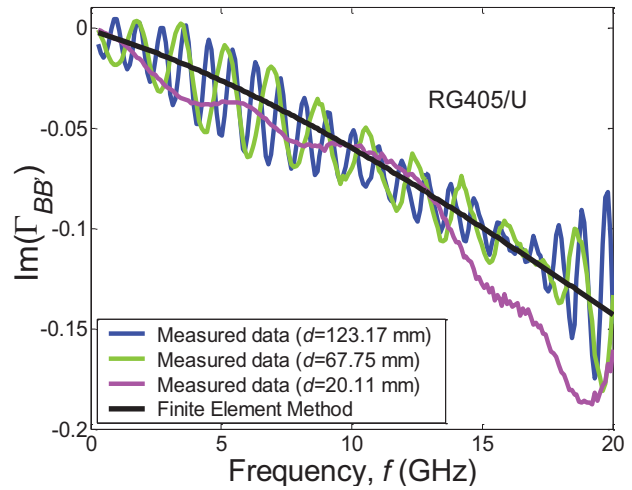


Fig. 10. Measured $\Gamma_{BB'}$ for air with considering standing wave for RG 405/U.

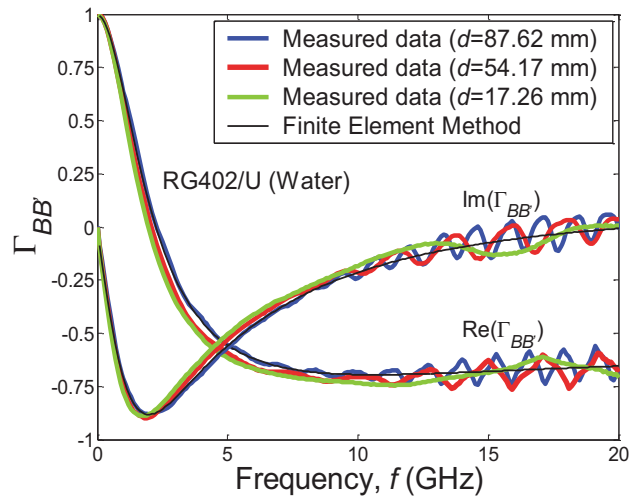


Fig. 11. Measured $\Gamma_{BB'}$ for water with considering standing wave for RG 402/U.

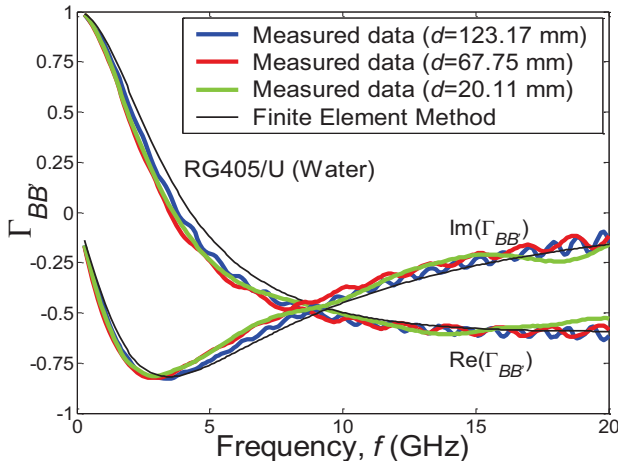


Fig. 12. Measured Γ_{BB} for water with considering standing wave for RG 405/U.

was removed compared to the measured results for air in Figs. 7 and 8. However, slight ripples still remain in the measurements due to the difficulty in obtaining a constant value of ρ_n^+ and ρ_n^- in (3b). The values of ρ_n^+ and ρ_n^- are affected by the gap between the inner and outer conductor. Unfortunately, this gap is a non-consistency over the coaxial length, due to the manufacturing tolerances - especially for RG405/U, which has a narrow coaxial gap. Moreover, the straightness and roundness for the coaxial line, as well as the flatness for the open end of the coaxial line, can also affect the values of ρ_n^+ and ρ_n^- . The average values for the first two terms of multiple reflection (ρ_o^+ , ρ_l^+ , ρ_o^- and ρ_l^-) for both sensors are given in Tab. 1.

4.4 Errors Analysis

In this section, the effects of standing waves on systematic measurement errors were analyzed. Fig. 13 shows an example of the standing wave effect on the imaginary part of the measured reflection coefficient of free space by using a 17.26 mm of RG402/U sensor. Fig. 13 (a) and (b) illustrates the $n=0$ and $n=1$ order standing wave, respectively over 300 MHz to 20 GHz. The values of the parameters in the standing wave calculations were taken from Tab. 1. In Fig. 13 (a) and (b), the red and blue lines are respectively representing the forward and backward multiple reflection, while the solid black line is the instantaneous magnitude of the standing wave results obtained from the sum of forward and reverse multiple reflection. The maximum amplitude of $n=0$ and $n=1$ orders of standing wave achieved 0.17 and 0.07, respectively. This means that the total magnitude of the standing wave in the 17.26 mm coaxial line will reach $(0.17 + 0.07) = 0.24$ at high operation frequencies as shown in Fig 3 (c). Clearly, the absolute error, $\text{Im}(\Gamma_{BB}) - \text{Im}(\Gamma_{FEM})$, for the imaginary part of measured reflection coefficient quite agrees with the calculated standing wave, as shown in Fig. 13(d). Hence, we can conclude that the effects of standing waves can cause up to 24 % relative error in the measured reflection coefficient by using the 17.26 mm RG402/U sensor.

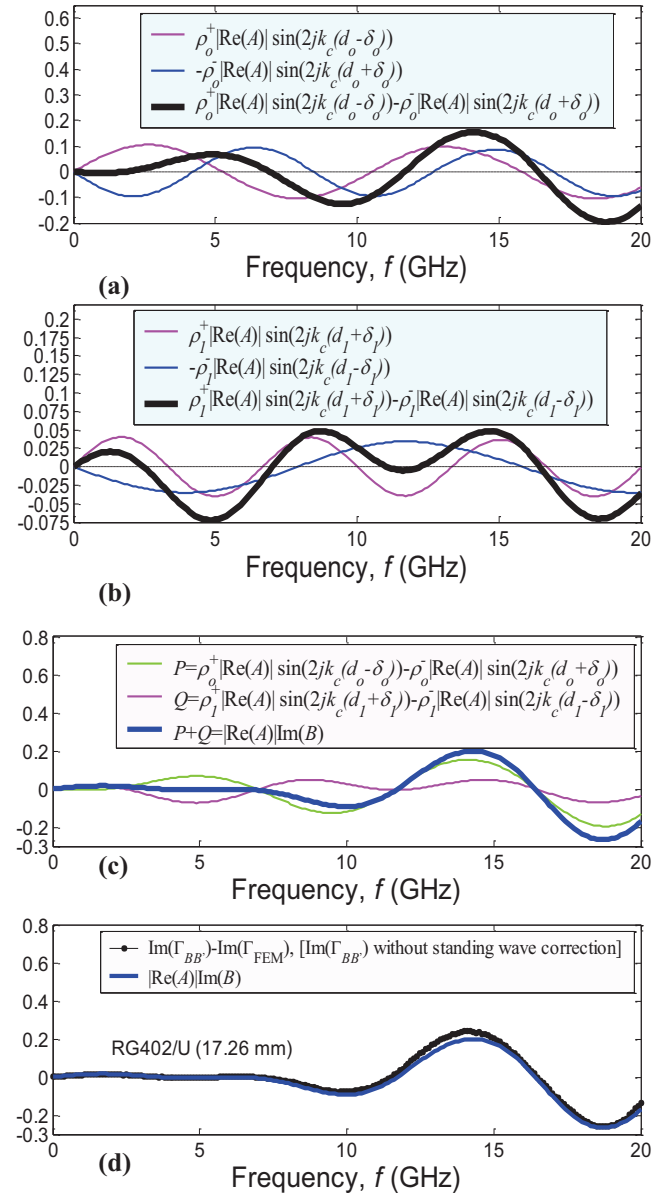


Fig. 13 (a) $n=0$ order instantaneous magnitude of standing wave (solid black line) results from sum of forward (red line) and reverse (blue line), (b) $n=1$ order instantaneous magnitude of standing wave (solid black line) results from sum of forward (red line) and reverse (blue line), (c) Total magnitude of standing wave (solid blue line) results from the combination of $n=0$ and $n=1$ orders standing wave, (d) Comparison between the total magnitude of standing wave and the absolute error for imaginary part of measured reflection coefficient from 300 MHz to 20 GHz.

Fig. 14 shows the absolute error for the imaginary part of the reflection coefficient, $\text{Im}(\Gamma_{BB}) - \text{Im}(\Gamma_{FEM})$ along the coaxial line for RG402/U sensor at 10 GHz. The absolute error is oscillated along the coaxial length, d , which is obeyed to the proposed standing wave calculation, $|\text{Re}(A)| \times \text{Im}(B)$. In Fig. 14, the values of $\text{Im}(\Gamma_{BB})$ do not take into account the standing wave effects and values of Γ_{AA} in (3a) obtained from FEM simulation.

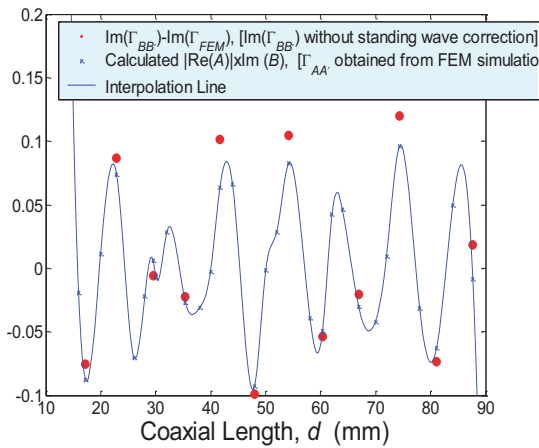


Fig. 14. Variational in absolute error of measured reflection coefficient with actual coaxial length, d for RG 402/U sensor at 10 GHz for free space.

5. Conclusions

In this work, the effects of coaxial length for the RG402/U and RG405/U coaxial probe have been intensively studied and reported. The calibration relationship between the measurement port and the aperture coaxial probe was successfully developed using a transmission approach.

Acknowledgements

This study was supported by the Fundamental Research Grant Scheme (FRGS) Phase 2/2009 from Ministry of Higher Education Malaysia under project number 78486.

References

- [1] ELLISON, W. J., MOREAU, J. M. Open-ended coaxial probe: model limitations. *IEEE Transaction on Instrumentation and Measurement*, 2008, vol. 57, no. 9, p. 1984 - 1991.
- [2] WONG, K. H. Using precision coaxial air dielectric transmission lines as calibration and verification standards. *Microwave Journal*, 1988, vol. 31, no. 12, p. 83 - 92.
- [3] BODNAR, D. G. Materials and design data. JOHNSON, R. C. (ed.) *Antenna Engineering Handbook*, 3rd edition. New York: McGraw-Hill, 1993.
- [4] Agilent Technologies Inc, USA. *Specifying Calibration Standards and Kits for Agilent Vector Network Analyzers*, Application Note 1287-11. 2010.
- [5] SORRENTINO, R., BIANCHI, G. *Microwave and RF Engineering*. Chichester (UK): Wiley, 2008.

Appendix

The exponential equation (4a) and (4b) can be separated into real and imaginary parts by using the terms of $\cos(x)$ and $\sin(x)$ as

$$\begin{aligned} F_0 &= \rho_0^+ \exp[2jk_c(d_0 - \delta_0)] = \\ &= \underbrace{\rho_0^+ \cos[2k_c(d_0 - \delta_0)]}_{\text{real part}} + \underbrace{j\rho_0^+ \sin[2k_c(d_0 - \delta_0)]}_{\text{imaginary part}} = \quad (\text{A.1}) \\ &= \text{Re}(F_0) + j \text{Im}(F_0), \end{aligned}$$

$$\begin{aligned} R_0 &= -\rho_0^- \exp[2jk_c(d_0 + \delta_0)] = \\ &= -\underbrace{\rho_0^- \cos[2k_c(d_0 + \delta_0)]}_{\text{real part}} + \underbrace{j\rho_0^- \sin[2k_c(d_0 + \delta_0)]}_{\text{imaginary part}} = \quad (\text{A.2}) \\ &= \text{Re}(R_0) + j \text{Im}(R_0). \end{aligned}$$

Fig. A1 shows the $n=0$ order imaginary part of forward, $\text{Im}(F_0)$ (red line) and reverse, $\text{Im}(R_0)$ (blue line) reflection along the RG402/U coaxial line at 1 GHz. The $\text{Im}(F_0)$ and $\text{Im}(R_0)$ are calculated using imaginary part of (A.1) and (A.2), respectively. The values of the parameters in (A.1) and (A.2) were taken from Tab. 1.

The corresponding vector phasor diagram for the $\text{Im}(F_0)$ and the reverse, $\text{Im}(R_0)$ at certain length, d of RG402/U coaxial line are shown in Fig. A2. Fig. A3 shows the total amplitude for imaginary part of standing wave coefficient (solid black line), results from the sum of the $\text{Im}(F_0)$ and the reverse, $\text{Im}(R_0)$ reflection for RG402/U sensor at 1 GHz.

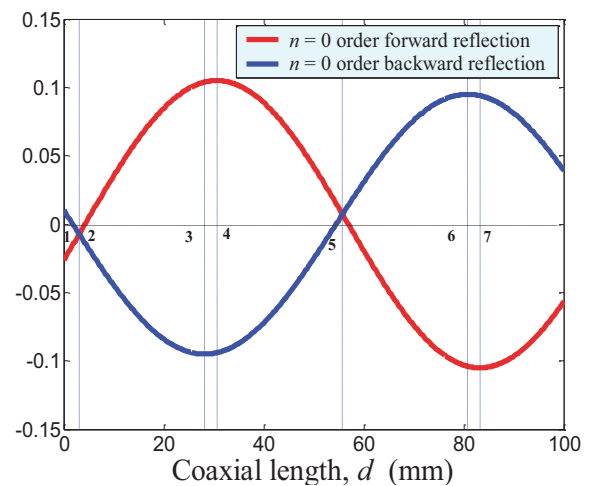


Fig. A1. the $n=0$ order imaginary part of forward, $\text{Im}(F_0)$ (red line) and reverse, $\text{Im}(R_0)$ (blue line) reflection along the RG402/U coaxial line at 1 GHz.

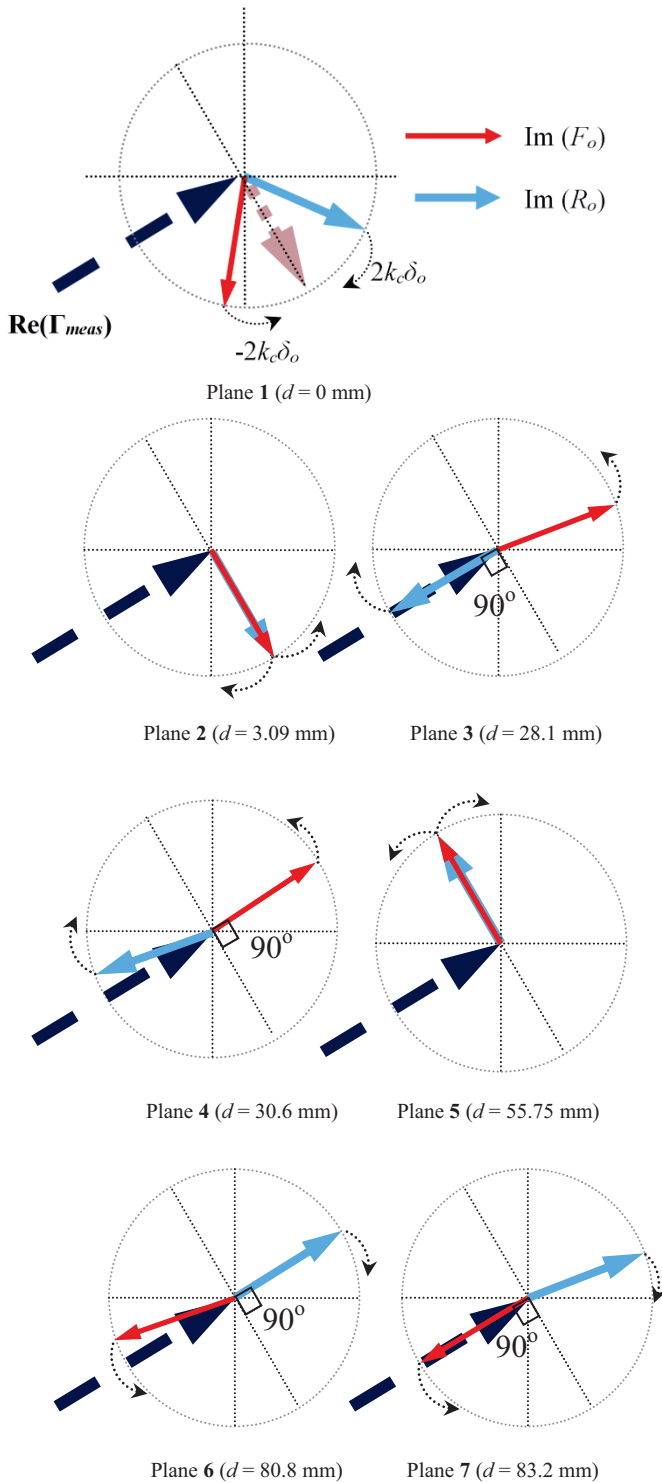


Fig. A2. Vector phasor diagram for the $\text{Im}(F_o)$ and the reverse, $\text{Im}(R_o)$ at certain length, d of RG402/U coaxial line.

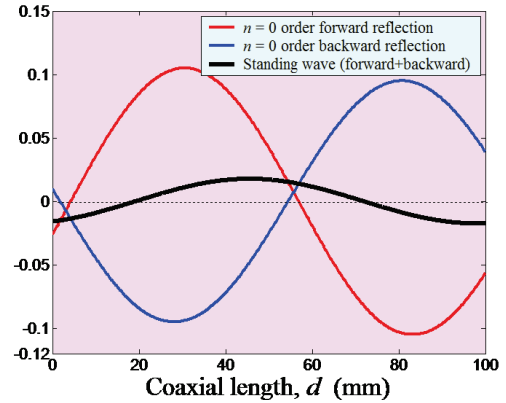


Fig. A3. Total amplitude for imaginary part of standing wave coefficient (solid black line), results from the sum of the $\text{Im}(F_o)$ and the reverse, $\text{Im}(R_o)$ reflection for RG402/U sensor at 1 GHz.

About Authors ...

K. Y. YOU was born in 1977. He obtained his B.Sc in Physics (Honours) degree in Universiti Kebangsaan Malaysia in 2001. He pursued his M. Sc. in Microwave at the Faculty of Science in 2003 and his Ph.D. in Wave Propagation at the Institute for Mathematical Research in 2006 in Universiti Putra Malaysia. Recently, he is a senior lecturer at Radio Communication Engineering Department, Universiti Teknologi Malaysia.

J. SALLEH was born in 1986. She received her B. Eng. (Telecommunication) from Universiti Teknologi Malaysia in 2009. Now, she is taking her Master in Microwave engineering field at same university.

Z. ABBAS was born in 1962. He obtained his B. Sc. Physics from Universiti Malaya in 1986. After that, he received his M. Sc. in Microwave in 1994 from Universiti Putra Malaysia and Ph. D in 2000 from University of Leeds in Microwave Instrument. Currently, he is senior lecturer at Department of Physic, Universiti Putra Malaysia.